Contact lines on soft solids with uniform surface tension: analytical solutions and double transition for increasing deformability

Julien Dervaux, Laurent Limat

Contact lines on soft solids with uniform surface tension: analytical solutions and double transition for increasing deformability.

Julien Dervaux[a,b], Laurent Limat[b]

[a]*Laboratoire Interdisciplinaire des Energies de Demain (LIED), UMR 8236 of CNRS and University Paris Diderot, 10 rue Alice Domon et Léonie Duquet, 75013 Paris, France*
[b]*Laboratoire Matière et Systèmes Complexes (MSC), UMR 7057 of CNRS and University Paris Diderot, 10 rue Alice Domon et Léonie Duquet, 75013 Paris, France.*

Abstract

Using an exact Green function method, we calculate analytically the substrate deformations near straight contact lines on a soft, incompressible solid, having a uniform surface tension γ_s. This generalized Flamant-Cerruti problem of a single contact line is regularized by introducing a finite width $2a$ for the contact line. We then explore the dependance of the substrate deformations upon the softness ratio l_s/a, where $l_s = \gamma_s/(2\mu)$ is the elastocapillary length built upon γ_s and on the elastic shear modulus μ. We discuss the force transmission problem from the liquid surface tension to the bulk and surface of the solid, and show that Neuman condition of surface tension balance at the contact line is only satisfied in the asymptotic limit $a/l_s \to 0$, Young condition holding in the opposite limit. We then address the problem of two parallel contact lines separated from a distance $2R$, and we recover analytically the "double transition" upon the ratios l_s/a and R/l_s identified recently by Karpitschka et al, when one increases the substrate deformability. We also establish a simple analytic law ruling the contact angle selection upon R/l_s in the limit $a/l_s \ll 1$, that is the most common situation encountered in problems of wetting on soft materials.

Keywords: Contact line, Wetting, Flamant-Cerruti

1. Introduction

Statics and dynamics of wetting of soft solids, that can be easily deformed by liquid surface tension, are presently motivating a renewed interest, via both experiments [1, 2, 3] and modeling [4, 5, 6, 7]. This interest is partly motivated by the huge number of applications of this field (soft condensing or desiccating coatings, artificial tissues, culture media, etc), but also by several underlying fundamental challenges that are still pending. As well known from ancient works [8, 9, 10, 11], a ridge is formed on the solid surface at the contact line and the interaction between the liquid surface and this ridge governs the selection of apparent contact angle [12], the possible hysteresis of this angle [13], and can also lead to very complex phenomena with unusual spreading laws [14], unstationary behaviors of contact lines [15, 3, 16, 17] or even instabilities with spatial pattern formation [18]. However, the precise structure of this ridge is still under debate [19], and for instance, it is only recently that the surface tension of these materials has been included in the modeling[5, 7, 4] in a way that could allow some direct comparisons with the more well known case of liquid/liquid wetting. The difficulties to reach a full theory are still numerous: how to build a reasonably simple formalism combining two different substrate surface tensions (for the wet and dry part of the surface [20]), finite deformations, substrate rheology and more generally dynamical effects?

In the present paper we focus on a simple case that allows us to perform analytical calculations of reasonable complexity. We consider statics with a simple liquid of surface tension γ deposited on a purely elastic, incompressible solid of infinite depth and of uniform elastic shear modulus μ. The substrate surface tension γ_s is supposed to be large compared to that of the liquid, which, as we shall see, will allows us to work in the small slope limit of the solid surface, i.e. in the limit of linear deformations of the bulk of the substrate. We will also simplify even more by neglecting any subtlety around the possible difference between substrate surface stress and substrate surface energy [21, 22], which seems to be a reasonable approximation in the case of incompressible media [23], and we will assume that the surface energy is the same for both the wet and dry parts of the substrate.

Email addresses: dervauxjulien@wanadoo.fr (Julien Dervaux), laurent.limat@univ-paris-diderot.fr (Laurent Limat)

This set of approximation may seem very reductive, but it is in fact the situation addressed by most recent available theoretical papers, and even this simple situation is imperfectly solved, as very often these approaches consider complex axisymmetric geometries involving numerical calculations. For instance Style and Dufresne [7] showed that in the large softness limit of sessile circular drops, of radius R, there are two different limits: when R is much larger than the elastocapillary length $l_s = \gamma_s/(2\mu)$, the situation at the contact line is very close to that of a liquid, with a Neumann condition of balance of surface tension at the contact line. In the opposite limit, one recovers rather the Young condition defining the equilibrium contact angle from a balance of forces in the horizontal direction. Very recently, Lubbers et al considered one or two contact lines of finite width a, and showed that this rigid to soft transition was in fact more complex, with two distinct transitions involving the two dimensionless parameters a/l_s and R/l_s, R being the radius of a drop or the half distance between two parallel contact lines [24].

In a previous paper [4] one of us developed a strategy to generalize the Green function used long ago by Shanahan et al [8, 9, 10], to a solid having a non-zero surface tension, and investigated the deformation field for one or two straight contact lines by using a simplified version of this Green function, while focusing mainly on the limit $R/l_s \gg 1$ of large softness. In the present paper, we reconsider this approach by using the exact Green function, and apply it to a single contact line of finite width, and also to two parallel contact lines of finite width for any values of the ratios l_s/a and R/l_s. We discuss the complexity of force transmission between the liquid surface tension and both the bulk and surface of the solid, and we derive analytical results for the slope of the solid and the selection of the liquid apparent contact angles. In particular, we show that the double transition found by Karpitcha et al can be in fact exactly calculated for any value of the contact angle. We then show that the selection of the apparent contact angles is dependent on geometrically nonlinear effects involving finite value of the substrate slope, which is out of reach of available analytical approaches. However, we give a simple analytical formula that should rule the selection of the contact angle for large l_s/a and l_s/R ratios. Again in the limit of large l_s/a ratio, an additional hypothesis motivated by the results contained in this paper allows us to suggest a more general formula for the selection of the contact angle for *arbitrary* l_s/R ratio.

In section 2, we first recall the limiting case of the Neumann and Young-Dupré relationships. In section 3 we remind the Green function approach developed in [4] for an incompressible solid, on the basis of an analogy with Stokes flows in hydrodynamics of viscous flows. We then solve the case of a single contact line of finite width $2a$. We provide an exact solution and extend the approximate solution developed in reference [4]. We show that, although not exact, it also leads to reasonable approximations for the calculated quantities in the present article. We then calculate the total elastic force beneath the contact line and we derive a macroscopic force balance at the contact line that reduces to the Neumann and Young-Dupré models in the appropriate limits. In section 4, we address the case of two parallel contact lines and explore in details the double transition, again for the exact and approximate Green function solutions. We derive several simple scaling laws for the substrate slope in the various regimes of interest. Because these results are valid for all contact angles, they can be used to describe the substrate deformations induced by a pinned drop in which the contact angle can take arbitrary values between two limits. We then address in section 5 the selection of the macroscopic drop contact angle when the contact line is not pinned. We show that energy minimization can predict this angle for large drops $l_s/R \ll 1$ on hard substrates $l_s/a \ll 1$. In the limit of soft substrates $l_s/a \gg 1$, nonlinear effects comes into play for contact angles close to $\pi/2$. We then show that these effect can be taken into account in the asymptotic limit of small drops $l_s/R \to \infty$ on soft substrate where we recover the Neumann construction. For drops of arbitrary sizes on soft substrates, we propose an analytic attempt to solve the apparent contact angle selection that avoids to use a complex minimization of free energy. We propose a simple formula linking the contact angle to the slope of the substrate deformation that should hold in the limit where $l_s/a \gg 1$.

2. General setting and the limiting cases of Young-Dupré and Neumann

Let us first consider a two-dimensional rivulet lying at the surface of an infinite, incompressible and linearly elastic half-space as illustrated in figure 5. The substrate is characterized by a Young modulus noted μ. As the problem is invariant along the z-coordinate, we shall assume that this surface loading creates a state of plane strain within the substrate. In response to the applied distribution of both normal and tangential surface forces $\vec{F} = \left\{F_x, F_y, 0\right\}$, elastic stresses build up within the solid and, if the free surface has a non-zero surface tension, surface forces also oppose the deformation. At the mechanical equilibrium, the deformation of the substrate at the contact line therefore results from the balance between loading, surface tension and elasticity. In the case of a liquid drop, the loading force is related to the surface tension γ_{LV} at the liquid-vapor interface and to the apparent contact angle θ_{LV} by the relation $\vec{F} = \{\gamma_{LV}\cos\theta_{LV}, \gamma_{LV}\sin\theta_{LV}, 0\}$. This force balance can be projected onto the x and y axis to yields:

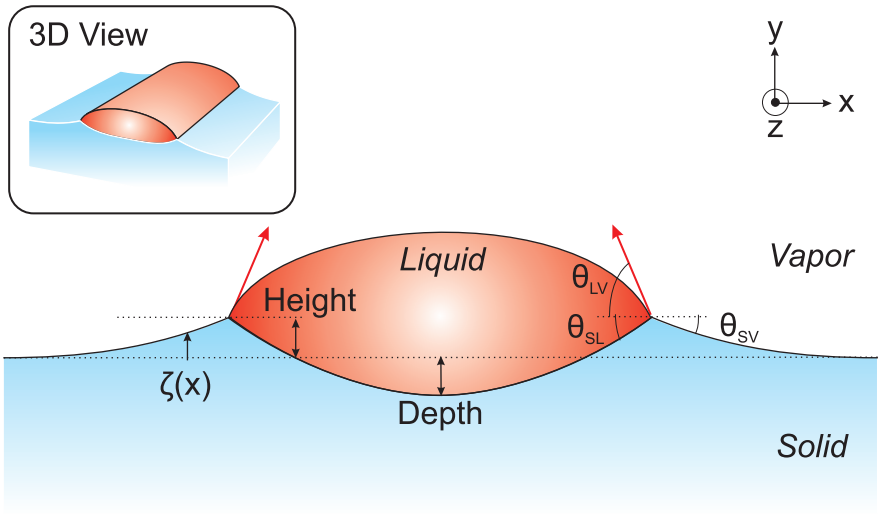

Figure 1: (color online). Schematic representation of the rivulet case. A 2D rivulet is lying on top of a linearly elastic half space with surface tension γ_s. The half-space is therefore subjected to two line forces at the corner of the rivulet and to a Laplace pressure beneath the drop.

$$\gamma_{LV}\cos\theta_{LV} = \gamma_{SL}\cos\theta_{SL} - \gamma_{SV}\cos\theta_{SV} + f_x^{\mathrm{el}} \quad (1)$$

$$\gamma_{LV}\sin\theta_{LV} = -\gamma_{SL}\sin\theta_{SL} - \gamma_{SV}\sin\theta_{SV} + f_y^{\mathrm{el}} \quad (2)$$

where f_x^{el} and f_y^{el} are respectively the x and y component of the elastic restoring forces (per unit of length) at the corners of the drop. The set of equations has two well-known and widely used simplifications. In the particular case of a hard substrate, the typical size of the substrate deformations are of the order of γ_{LV}/μ ($\sim 10^{-12}$ m for water on glass) which is much smaller than the typical size R of droplets. Consequently, elastic deformations are neglected at large scale and the angles θ_{SL} and θ_{SL} are set to zero. In addition, elastic forces are also neglected from the horizontal force balance above and, in this approximation, the contact angle θ_{LV} is a solution of the simplified equation $\gamma_{LV}\cos\theta_{LV} + \gamma_{SL} - \gamma_{SV} = 0$. This balance of surface tensions at the triple line is known as the Young-Dupré equation and states that elastic stresses do not contribute to the selection of the contact angle. Because the contact angle, which is often the quantity of interest in wetting problems, is fully determined by this equation, the vertical force balance between surface tractions and elastic stresses is typically left unsolved. In the opposite limit of an infinitely soft substrate (a liquid at rest), the elastic stresses are set to zero: $f_x^{\mathrm{el}} = f_y^{\mathrm{el}} = 0$ and equantions (1)-(2) reduce to those considered by Neumann and followers [25, 26, 27]

Table 1: Summary of the force balance in the Young-Dupré and Neumann limit for arbitrary deformations.

	Horizontal force balance $\gamma_{LV}\cos\theta_{LV} =$	Vertical force balance $\gamma_{LV}\sin\theta_{LV} =$
hard substrate (Young-Dupré)	$\gamma_{SV} - \gamma_{SL}$	f_y^{el} *(typically not solved)*
soft substrate (Neumann)	$\gamma_{SL}\cos\theta_{SL} - \gamma_{SV}\cos\theta_{SV}$	$-\gamma_{SL}\sin\theta_{SL} - \gamma_{SV}\sin\theta_{SV}$

As can be seen in the table above, both theories lead to simple and elegant predictions as elastic stresses need not be calculated. Despite their ever-increasing applications, the wetting of gels is not covered by any of these two

theories as the capillary length, defined here as $2\gamma_s/\mu$ of gels can approach the typical sizes R of liquid drops. With this consideration in mind, this paper makes no assumption on the ratio of the capillary length over the size R of the droplets. Furthermore, we do not postulate *a priori* any "macroscopic force balance" such as (1)-(1). Instead, general boundary conditions are applied all over the free surface and we will derive this force balance by integrating the elastic stresses over the width of the contact line. We will then show analytically that the elastic stresses indeed vanish from these force balance in some limiting cases. For the sake of simplicity, we will consider from now on that the surface tensions γ_{SL} and γ_{SV} are equal and we write $\gamma_{SL} = \gamma_{SV} = \gamma_S$.

3. The single 2D contact line

3.1. Notations and general equations

Within this framework, the mechanical equilibrium in the bulk of the incompressible half-space is described by the Navier equations:

$$\nabla \cdot \vec{u} \tag{3}$$

$$\mu \triangle \vec{u} - \vec{\nabla} P = 0 \tag{4}$$

where $\vec{u}$ is the displacement field and P is the pressure field. This field is introduced as a Lagrange multiplier to enforce the incompressibility constraint. This set of equations is completed by the condition of stress continuity at the boundary:

$$\boldsymbol{\sigma} \cdot \vec{n} = \vec{t} \tag{5}$$

where $\vec{n}$ and $\vec{t}$ are the unit normal vector to the surface and traction forces exerted at the substrate boundary, respectively. In component form, the stress tensor $\boldsymbol{\sigma}$ is given by:

$$\sigma_{ij} = \mu \left(\frac{\partial u_i}{\partial x_j} + \frac{\partial u_j}{\partial x_i} \right) - P \delta_{i,j} \tag{6}$$

where $\delta_{i,j}$ is the Kronecker delta symbol.

3.2. The Green function

Let us first consider the problem introduced and solved by Limat [4], of a line force $\vec{f} = (f_x \delta(x)\delta(y), f_y \delta(x)\delta(y), 0)$ applied at the free boundary of a solid with surface tension γ_S. In order for the linear elastic theory to be valid, the slope of the surface profile $\zeta(x)$ must be small everywhere, i.e $\zeta'(x) \ll 1$ where the prime denotes the derivative with respect to x. Within this approximation, the boundary condition (5) takes the form:

$$\sigma_{yy} = 2\mu \frac{\partial u_y}{\partial y} - P = f_y \delta(x) + \gamma_S \frac{\mathrm{d}^2 \zeta}{\mathrm{d}x^2} \tag{7}$$

$$\sigma_{xy} = \mu \left(\frac{\partial u_y}{\partial x} + \frac{\partial u_x}{\partial y} \right) = f_x \delta(x) \tag{8}$$

This problem can be solved by using a potential function for the displacement field and working in Fourier space. The solution is given by:

$$u_y(x, y = 0) = \zeta(x) = \frac{f_y}{2\pi\mu} \int_{1/\Delta}^{\infty} \frac{\cos kx}{k + \frac{\gamma_S}{2\mu} k^2} \mathrm{d}k \tag{9}$$

$$u_x(x, y = 0) = \frac{f_x}{2\pi\mu} \int_{1/\Delta}^{\infty} \frac{\cos kx}{k} \mathrm{d}k \tag{10}$$

where Δ is a macroscopic cut-off length (we will come back to this point later on). Performing the integrals yields the following expression for the displacement field:

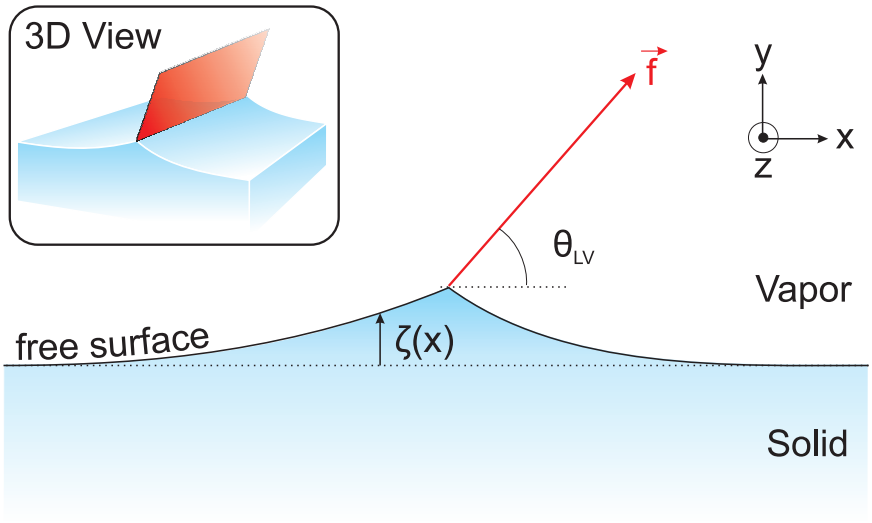

Figure 2: (color online). Schematic representation of the problem. A linearly elastic half space is subjected to a line force $\vec{f}$ at the origin of the free surface.

$$\zeta(x) = \frac{f_y}{2\pi\mu}\left\{-\mathrm{Ci}\frac{|x|}{\Delta} + \cos\frac{|x|}{l_s}\mathrm{Ci}\left(\frac{|x|}{\Delta}+\frac{|x|}{l_s}\right) + \sin\frac{|x|}{l_s}\left(\mathrm{Si}\left(\frac{|x|}{\Delta}+\frac{|x|}{l_s}\right)-\frac{\pi}{2}\right)\right\} \tag{11}$$

$$u_x(x, y=0) = \frac{f_x}{2\pi\mu}\left\{-\mathrm{Ci}\frac{|x|}{\Delta}\right\} \tag{12}$$

and $l_s = \gamma_s/2\mu$ is the capillary length of the solid. Up to a constant and far from the cut-off length ($x \ll \Delta$), the solution above can be slightly simplified to:

$$\zeta(x) = \frac{f_y}{2\pi\mu}\left\{-\log\frac{|x|}{\Delta} + \cos\frac{|x|}{l_s}\mathrm{Ci}\frac{|x|}{l_s} + \gamma + \sin\frac{|x|}{l_s}\left(\mathrm{Si}\frac{|x|}{l_s}-\frac{\pi}{2}\right)\right\} = \frac{f_y}{2\pi\mu}H(x) \tag{13}$$

$$u_x(x, y=0) = \frac{f_x}{2\pi\mu}\left\{-\log\frac{|x|}{\Delta}\right\} = \frac{f_x}{2\pi\mu}G(x) \tag{14}$$

where $\gamma \approx 0.577$ is the Euler-Mascheroni constant. Note that the normal (resp. horizontal) component of the displacement field depend only on the normal (resp. horizontal) component of the applied surface force. As a consequence, only the deflection ζ of the surface depends on the surface tension of the solid. The absence of coupling between horizontal displacement and vertical loading is a characteristic feature of a linear incompressible half-space. In the limit $ls \to 0$, we recover the solution of the Flamant-Cerruti problem [28, 29]. Note that these expressions diverge both at large and small x. The divergence of the displacement field at large distance from the drop is solely a consequence of the 2D character of the problem (similar to the logarithmic divergence of the flow field past a cylinder in 2D hydrodynamics) and can be regularized, for example, by formulating the problem in 3D. The divergence of the displacement near $x = 0$ on the other hand, follows from the localized nature of the applied force. While this solution might be a reasonable description at some distance (to be specified later) from the contact line, this description must break down at smaller scales. At the lengthscale of the gel correlation length (typically 1 nm), the structure becomes heterogeneous and the continuous model indeed does not hold. Irregularities may also arise from the roughness of the free surface at a larger scale, as sen on figure 3. Because of these defects, real contact lines have some ”thickness” in the sense that the triple line is pinned to the defects and oscillates within a narrow band of width $2a$. Before applying this regularization at small scales, let us first note that the Green function above can also be reasonably approximated by another simpler function.

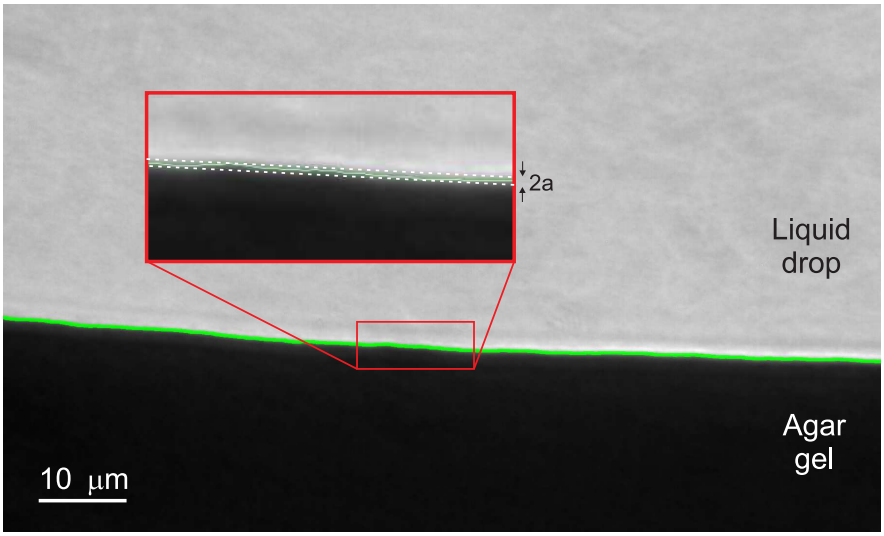

Figure 3: (color online). Detail of a triple line at the boundary of a water drop on a soft agar gel (1.5% agarose). The boundary is highlighted by a green line and the inset shows the oscillation of the triple line resulting from the heterogeneities at the surface of the gel. The contact line oscillate within a narrow band whose width is of order of a micrometer.

3.3. A simplified Green function

In the limit $l_s \to 0$ (with $x \ll ls$), the solution $\zeta(x)$ above and its first derivative $\theta(x) = \zeta'(x)$ has the following asymptotic form:

$$\zeta(x) = -\frac{f_y}{2\pi\mu}\left(\gamma + \log\frac{|x|}{\Delta}\right) \text{ and } \theta(x) = -\frac{f_y}{2\pi\mu}\frac{1}{|x|} \tag{15}$$

$$u_x(x, y = 0) = -\frac{f_x}{2\pi\mu}\log\frac{|x|}{\Delta} \tag{16}$$

while in the limit $x \to 0$ (and under the assumption that $l_s \ll \Delta$) the solution converges toward:

$$\zeta(x) = -\frac{f_y}{2\pi\mu}\log\frac{l_s}{\Delta} \text{ and } \theta(x) = -\frac{f_y}{2\pi\mu}\frac{\pi}{2l_s} \tag{17}$$

$$u_x(x, y = 0) = -\frac{f_x}{2\pi\mu}\log\frac{|x|}{\Delta} \tag{18}$$

In order to make further analytical progress, Limat [4] introduced the approximate solution $\tilde{\zeta}, \tilde{u_x}$:

$$\tilde{\zeta}(x) = -\frac{f_y}{2\pi\mu}\left(\gamma + \log\frac{|x| + 2l_s/\pi}{\Delta}\right) \tag{19}$$

$$\tilde{u_x}(x, y = 0) = -\frac{f_x}{2\pi\mu}\log\frac{|x|}{\Delta} \tag{20}$$

While the solution above is not exact, it is an interpolation between the limiting cases of the first derivative of the exact Green function. It also describes the far field ($x \ll ls$) behavior of the displacement field but fail to accurately predict the value of the deflection beneath the line load. As we shall see below by comparing the results obtained with this interpolation and the exact solution, it essentially captures the physics of the wetting on a soft substrate while greatly simplifying the calculations. In a previous paper, this solution was used: 1) to derive approximate solutions for the single and double (rivulet) contact line problem, 2) to give analytical predictions for the contact angles near the contact line as well as 3) for the amplitude of the substrate in the limiting case $R \gg l_s$ and 4) to build approximate methods for the experimentally-relevant case $\gamma_{SV} \neq \gamma_{SL}$.

3.4. Finite width of the contact line

In order to regularize the Flamant-Cerruti problem [28, 29] with surface tension formulated above, we now assume that the force acting on the substrate is spread out on a strip of width $2a$. The resulting displacement field on the surface $(\zeta^a(x), u_x^a(x, y = 0))$ can be readily obtained by using $f_y = \Pi_y \mathrm{d}y$ and $f_x = \Pi_x \mathrm{d}y$ and by integrating the previous result. Since we are mostly interested by the angles at the contact line, we only present here the analytical result for the slope $\theta_a(x) = \zeta'^a(x)$ of the surface deflection:

$$\theta^a(x) = \frac{\Pi_y}{2\pi\mu} \int_{-a}^{a} \mathrm{d}y H'(x-y) = -\frac{\Pi_y}{2\pi\mu} \{H(x-a) - H(x+a)\} \tag{21}$$

where $H(x)$ was introduced in equation (13). The analytical solution for $\zeta^a(x)$ itself is given in appendix and plotted in figure 4, along with the solution $\zeta(x)$ (i.e. in the limit $a \to 0$) as well as the correspond solutions obtained with the simplified Green function ($\tilde{\zeta}(x)$ and $\tilde{\zeta}^a(x)$, which expression can be found in section V). As expected, the slope of the surface deflection does not depend on the macroscopic cut-off anymore. Evaluating this expression on either side of the contact strip we find the contact angle $\theta^a(-a) = -\theta^a(a)$:

$$\theta^a(-a) = \frac{\Pi_y}{2\pi\mu} \left\{ \log\left(\frac{2a}{l_s}\right) + \gamma - \mathrm{Ci}\frac{2a}{l_s} \cos\frac{2a}{l_s} + \frac{1}{2}\left(\pi - 2\mathrm{Si}\frac{2a}{l_s}\right) \sin\frac{2a}{l_s} \right\} \tag{22}$$

It is instructive to compare this behavior with known results for hard ($\mu \gg \gamma_{LV}/a, \gamma_s/a$) and soft substrates ($\mu \ll \gamma_{LV}/a, \gamma_s/a$). Writing the normal force $\Pi_y = (\gamma_{LV} \sin\theta_{LV})/(2a)$, the contact angle has the following simple asymptotic behaviors in these limits:

$$\theta^a(-a) \sim \underbrace{\frac{\gamma_{LV}\sin\theta_{LV}}{\gamma_s}}_{\theta_{ref}} \begin{cases} \dfrac{1}{2}\left(1 + \dfrac{2a}{l_s\pi} \log\dfrac{2a}{l_s}\right) & \text{soft substrate} \\ \dfrac{l_s}{2a\pi} \log\dfrac{2a}{l_s} & \text{hard substrate} \end{cases} \tag{23}$$

On a soft substrate, the contact angle, at leading order, is independent of the substrate stiffness and we recover the value given by the Neumann triangle construction for a liquid droplet on a liquid substrate (in the limit of small angle, as linear elasticity is only valid for small slopes). When the substrate becomes stiffer, the contact angle decreases and behaves as $\sim \log(\mu)/\mu$ at large μ. In the limit of an infinitely stiff substrate, the angle goes to zero and we recover the Young's model in which the substrate remains flat. This prediction is in sharp contrast with the result of Style and Dufresnes [7], where the substrate angle is always given by Neumann's law close to the ridge and by the Young's law far from the ridge. Within our framework, there is no "liquid-like" behavior near the ridge and the value of the substrate angle at the contact line depends essentially on the ratio of the elastocapillary length to the width of the contact line l_s/a.

3.5. Force balance at the contact line

We now take advantage of our analytical solution to investigate the force balance at the contact line. In the elastic substrate subject to a line force, the normal component of the stress tensor on the upper surface ($y = 0$) is given by:

$$\sigma_{yy}(x, y = 0) = \frac{f_y}{\pi} \int_{1/\Delta}^{\infty} \frac{\cos kx}{1 + \frac{\gamma_s}{2\mu}k} \mathrm{d}k \tag{24}$$

In the case of a force applied on a strip with a finite width, the stress $\sigma_{yy}^a(x)$ at the surface is given by:

$$\sigma_{yy}^a(x) = \frac{\Pi_y}{f_y} \int_{-a}^{a} \mathrm{d}y \sigma_{yy}(x-y) = \frac{\Pi_y}{\pi} \{J(x-a) - J(x+a)\} \tag{25}$$

where

$$J(x) = -\left\{ \cos\frac{x}{l_s}\mathrm{Si}\frac{x}{l_s} - \sin\frac{x}{l_s}\mathrm{Ci}\frac{|x|}{l_s} + \pi \sin\frac{|x|}{2l_s} \sin\frac{x}{2l_s} \right\} \tag{26}$$

Integrating the stress over the width of the strip, we find the total line force f_y^{el} in the substrate below the contact line:

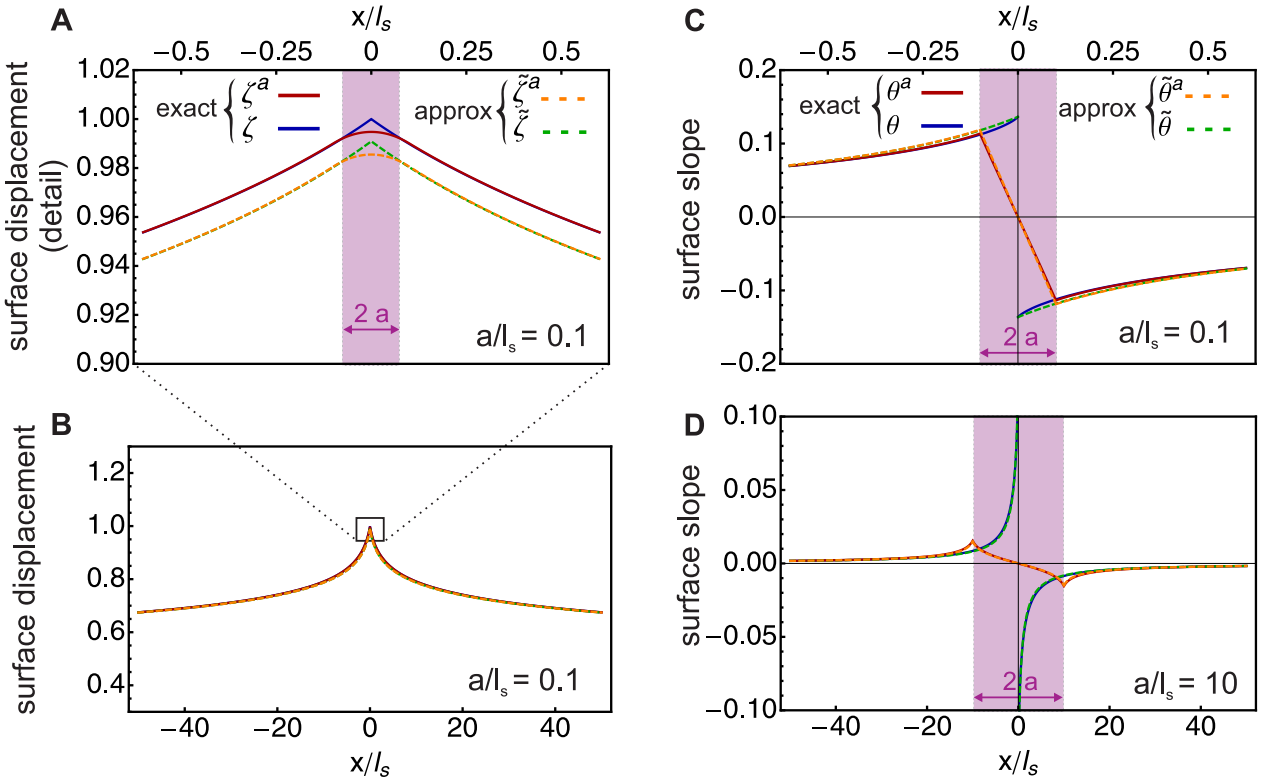

Figure 4: Surface displacement fields close (top) and far (bottom) from the contact line. The exact solutions are shown for both the line loading (solid blue line) and the narrow strip of width $2a$ (solid red line). For comparison, we also plot the corresponding results for the approximate solutions $\zeta(x)$ defined in (dashed green line) as well as $\zeta^a(x)$ defined in (dashed orange line). Displacement have been normalized such that the maximum value of the exact solution is 1 at $x = 0$. Parameter values are $a = 1/10$, $\Delta = 10^5$.

$$f_y^{el} = \int_{-a}^{a} \mathrm{d}x \sigma_{yy}^a(x) = \frac{2l_s\Pi_y}{\pi}\left\{\mathrm{Ci}\frac{2a}{l_s}\cos\frac{2a}{l_s} - \left(\frac{\pi}{2} - \mathrm{Si}\frac{2a}{l_s}\right)\sin\frac{2a}{l_s} + \frac{\pi a}{l_s} - \log\frac{2a}{l_s} - \gamma\right\} \tag{27}$$

Using expression (22) as well as the expression for Π_y, one may recognize:

$$f_y^{el} = \gamma_{LV}\sin\theta_{LV} - 2\gamma_s\theta^a(-a) \tag{28}$$

This relation is the macroscopic force balance (2) in the limit of small substrate deformation and symmetric surface tension. It can also be obtained by direct integration of the boundary condition (8). The first term is the integral of the normal traction applied at the surface and the second term is the integral of the Laplace pressure in the solid due to the curved interface. In the case of a single contact line with symmetric surface energies (i.e, on both sides of the contact line), the tangential component of the stress tensor integrated over the width of the leading strip, noted f_x^{el} is given by:

$$f_x^{el} = \int_{-a}^{a} \mathrm{d}x \sigma_{xy}^a(x) = \gamma_{LV}\cos\theta_{LV} \tag{29}$$

At the "macroscopic level" because the same line tension applies to both sides of the contact line the projection of the force γ_{LV} is only balanced by elastic stresses that develop in the substrate and the Neumann or Young-Dupré law are only recovered in the limit $\theta_{LV} \to \pi/2$. If the contact line is pinned to the surface however, the tangential elastic stress does not vanish and the contact angle can deviate from $\pi/2$, that is the "normal" value for $\gamma_{SL} = \gamma_{SV} = \gamma_s$. Looking at the asymptotic value of $\theta^a(a)$ presented above, one may notice that :

$$f_y^{el} \sim \gamma_{LV}\sin\theta_{LV}\begin{cases} \dfrac{2a}{\pi l_s}\log\dfrac{2a}{l_s} & \text{soft substrate} \\ 1 + \dfrac{l_s}{\pi a}\log\dfrac{2a}{l_s} & \text{hard substrate} \end{cases} \tag{30}$$

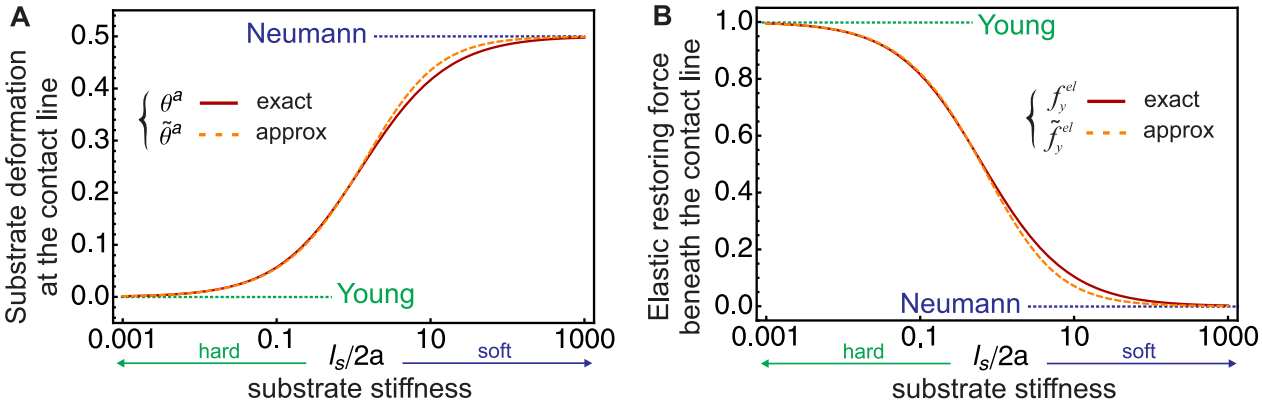

Figure 5: (color online). Substrate slope at the contact line (A) and total elastic force under the contact line (B) as a function of the dimensionless parameter $l_s/(2a)$. The angles are scaled by $\theta_{ref} = \gamma_{LV} \sin\theta_{LV}/\gamma_s$ and the total elastic force by $\gamma_{LV} \sin\theta_{LV}$. We plot the exact solution given by equation (22) as well as the approximate solution given by equation (43). The Young-Dupré and Neumann theories are recovered in the limits of hard ($l_s/(2a) \to 0$) and soft ($l_s/(2a) \to \infty$) substrate, respectively

On a soft substrate, the total normal stress at the surface below the triple line goes to zero in the limit where $2a/l_s \to 0$ and therefore elastic stress do not contribute to the local mechanical equilibrium at the contact line. The normal traction is balanced solely by interfacial stresses and we recover the small angle limit of the "macroscopic" force balance (shown in Table 1) as written by Neumann:

$$\gamma_{LV} \sin\theta_{LV} = 2\gamma_S \theta^a(-a) \text{ when } \frac{2a}{l_s} \to 0 \tag{31}$$

On a hard substrate on the other hand, the substrate slope goes to zero. As a consequence, the surface cannot deform enough to allow the previous force balance (31) to be satisfied and the contribution of the normal projection of the substrate surface tension becomes negligible. Instead, the traction exerted on the substrate at the contact line is only balanced by the elastic stresses that develop in the bulk of the substrate.

$$f_y^{el} = \gamma_{LV} \sin\theta_{LV} \text{ when } \frac{2a}{l_s} \to \infty \tag{32}$$

To leading order the equation above is the normal force balance in the Young-Dupré limit. This equation is typically left aside and only the horizontal force balance is written in standard theories of wetting on hard substrates.

4. The 2D rivulet

4.1. Contact angles

We now consider a liquid rivulet on an infinite, linearly elastic, half-space, as illustrated in figure 5. The rivulet has width 2R and deforms the substrate because of 1) the tractions at the two contact lines and 2) the Laplace pressure beneath the drop. Mechanical equilibrium in the drop requires the pressure P to be a constant given by Laplace law $P = \gamma_{LV} \sin\theta_{LV}/R$. The two contact lines are located at $-R$ and R and the surface slope is given by the following integral:

$$\theta^{a2D}(x) = \frac{\Pi_y}{2\pi\mu}\left\{\int_{-R-a}^{-R+a} dy H'(x-y) + \int_{R-a}^{R+a} dy H'(x-y)\right\} - \frac{P}{2\pi\mu}\int_{-R}^{R} dy H'(x-y) \tag{33}$$

$$= \frac{\Pi_y}{2\pi\mu}\{H(x+R+a) + H(x-R+a) - H(x+R-a) - H(x-R-a)\}$$

$$- \frac{P}{2\pi\mu}\{H(x+R) - H(x-R)\} \tag{34}$$

Note that in the case of a 2D rivulet (or an axisymmetric drop), the total force exerted on the substrate is zero. As a consequence, the surface of the substrate becomes flat far from the drop (see figure 6) and there is no divergence of

the deflection at infinity as it is the case for a single contact line. In the case of finite droplet size and finite width of the contact line, the Cerruti-Flamant problem is thus fully regularized. From the expression for the displacement field $\zeta^{a2D}(x)$ (given in appendix), we can therefore now plot the maximum height (at the corner of the drop, i.e $\zeta^{a2D}(R)$) and maximum depth (at the center of the drop, i.e $\zeta^{a2D}(0)$) of the substrate deformation in figure 6-B. While the depth of of the deformation increase monotonously with increasing softness of the substrate, the height of the substrate deformation exhibits a non-monotonous behavior. When the capillary length is below the width of the drop, the maximum height of the drop first increases and reaches a maximum when the capillary length is of order of the drop size $l_s \sim R$. For even softer substrate (or, equivalently, smaller droplets) the maximum height then decreases. Combined with the increase in depth of the substrate deformation, this indicates that the drop "sinks" within the substrate. Ultimately, both the depth and and height of the substrate saturate at finite values.

4.2. Double transition

The values of the contact angles on the wet θ_{SL} and the dry θ_{SV} side of the triple line are defined as:

$$\theta_{SL} \equiv \theta^{a2D}(R-a) \tag{35}$$

$$\theta_{SV} \equiv -\theta^{a2D}(R+a) \tag{36}$$

Note that with this definition, both the wet θ_{SL} and the dry angle θ_{SV} are positive. These angles can be written in a more compact form as a function of the geometric $A = a/R$ and elastic $B = l_s/R$ parameters (expression are given in annex). Their variations are shown in figure 6. In the limiting case of a very large drop ($a/R, l_s/R \ll 1$), we recover the limiting case of a single contact line described previously: i) on a hard substrate ($l_s/R \ll a/R$) the drop sits on the surface without deforming it and both angles, θ_{SL} and θ_{SV}, are equal to zero while ii) on a soft substrate ($a/R \ll l_s/R \ll 1$) both angles are equal to $\gamma_{LV}\sin\theta_{LV}/2\gamma_s$. In this case, the ridge is symmetric and the deformation is dominated by the traction exerted at the corners of the rivulet.

In the case of a smaller drop on the other hand, the capillary length is not negligible anymore compared to the radius of the drop (i.e $l_s \gtrsim R$) and a third regime appears in which the dry angle goes to zero while the wet angle increases to $\gamma_{LV}\sin\theta_{LV}/\gamma_s$. The ridge rotates towards the interior of the drop and the drop "sinks" inside the gel. in this case the deformation is strongly influence by the Laplace pressure in the drop acting on the substrate. These two transitions between the three regimes can also be made more obvious by plotting the sum and difference between the dry and wet angles. In the experimentally relevant case where $A = a/R \ll 1$, the following analytical expression for the sum and difference:

$$\frac{\pi(\theta_{SL}+\theta_{SV})\gamma_s}{\gamma_{LV}\sin\theta_{LV}} = \frac{B}{2A}\left\{2\left(\log\frac{2A}{B}+\gamma\right) - 2\mathrm{Ci}\frac{2A}{B}\cos\frac{2A}{B} + \left(\pi - 2\mathrm{Si}\frac{2A}{B}\right)\sin\frac{2A}{B}\right\} \tag{37}$$

$$\begin{aligned}\frac{\pi(\theta_{SL}-\theta_{SV})\gamma_s}{\gamma_{LV}\sin\theta_{LV}} =& -\sin\frac{2}{B}\left\{2\mathrm{Ci}\frac{2}{B} + 2B\mathrm{Si}\frac{2}{B} - \pi B\right\} - \cos\frac{2}{B}\left\{2B\mathrm{Ci}\frac{2}{B} - 2\mathrm{Si}\frac{2}{B} + \pi\right\} \\ &+ 2B(\gamma + \log\frac{2}{B})\end{aligned} \tag{38}$$

In this limit, the sum of the angles is the signature between a sitting to a pulling mode. This transition essentially depends on the ratio $B/A = l_s/a$. When the elastocapillary length (i.e the characteristic extent of the elastic deformation of the substrate) is smaller that the typical width of the triple line (hard sustrate), there are virtually no deformation of the surface and the drop sits on a flat interface. When the stiffness of the underlying substrate decreases, it is deformed by the normal projection of the liquid-vapor interfacial traction. Because l_s is still much smaller than the radius of the drop in this regime, the two triple lines are essentially non-interacting and the angle sum is just twice the single line value $\gamma_{LV}\sin\theta_{LV}/2\gamma_s$. This sitting-to-pulling transition can also be approximated by two simple scaling laws that may be easier to manipulate than the expressions above:

$$\theta_{SL}+\theta_{SV} \sim \frac{\gamma_{LV}\sin\theta_{LV}}{\gamma_s}\begin{cases} \dfrac{l_s}{\pi a}\log\dfrac{2a}{l_s} & \text{hard substrate} \\ 1+\dfrac{2a}{\pi l_s}\log\dfrac{2a}{l_s} & \text{medium substrate}\end{cases} \tag{39}$$

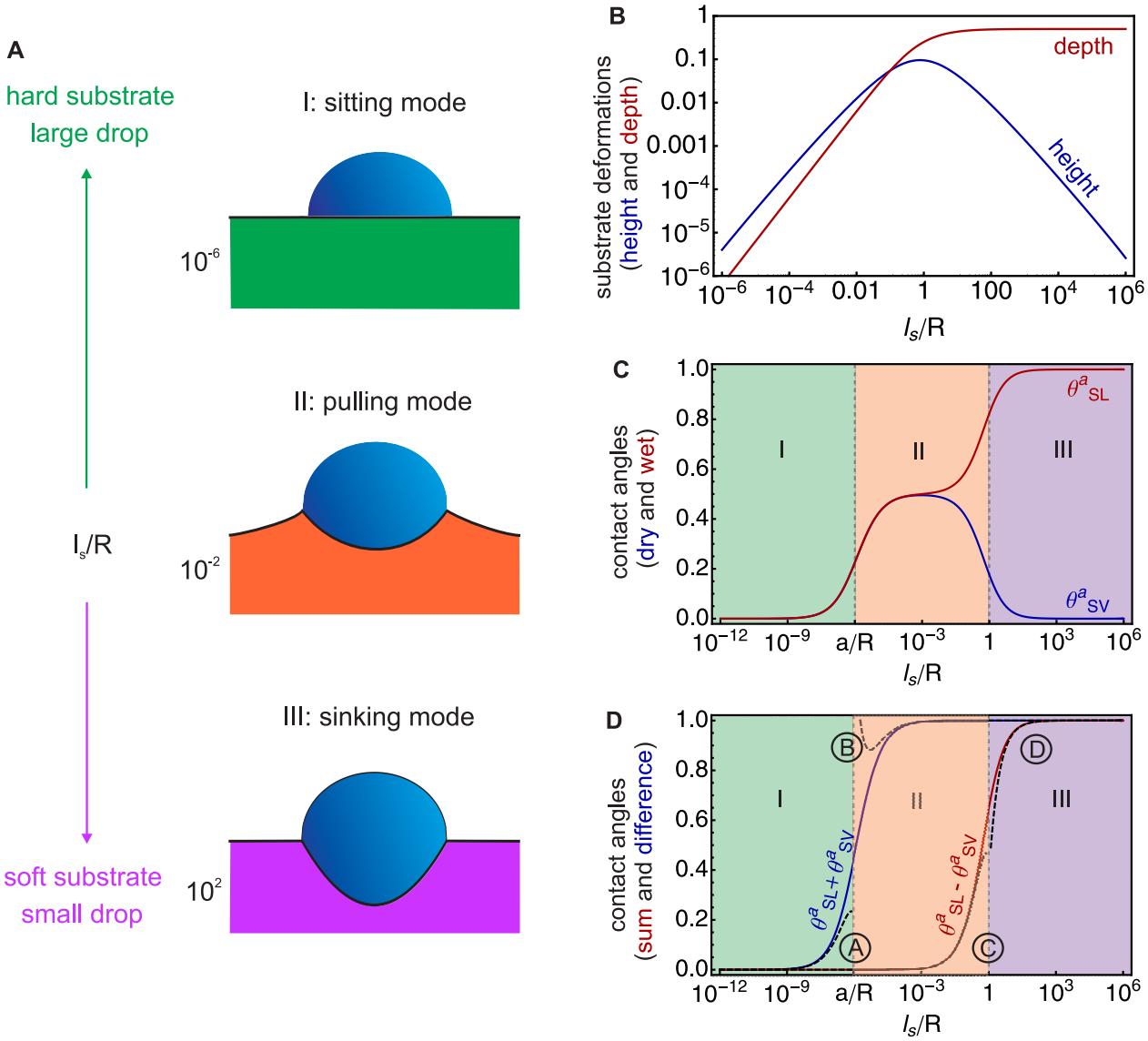

Figure 6: A) Deformation of the substrate for increasing deformability. The surface displacement field is given by equation (69. The amplitude is arbitrarily large for the purpose of illustration. B) Maximum height (given by $\zeta^{a2D}(R)$) and depth (given by $\zeta^{a2D}(0)$) of the substrate deformation. C) Dry (θ_{SV}) and wet (θ_{SL}) angles at the contact line. D) Sum and difference of the substrate contact angles scaled by $\gamma_{LV}\sin\theta_{LV}/\gamma_s$.

When the stiffness of the substrate underneath the drop further decreases (still in the limit where A is small), the capillary length becomes of a size of the order of the drop radius. The two contact lines start interacting and the Laplace pressure breaks the wet/dry symmetry of the ridge. As seen on figure 6, the ridges below the contact lines rotate until the dry interface becomes flat. The difference between the angles is now the key parameter controlling the transition from pulling to sinking mode and essentially depends on $B = l_s/R$, i.e the ratio of the elastocapillary length l_s over the radius of the drop. The pulling-to-sinking transition can also be approximated by two simple scaling laws:

$$\theta^a_{SL} - \theta^a_{SV} \sim \frac{\gamma_{LV}\sin\theta_{LV}}{\gamma_s}\begin{cases} \dfrac{2l_s}{\pi R}\log\dfrac{2R}{l_s} & \text{medium substrate} \\ 1 - \dfrac{2R}{\pi l_s} & \text{soft substrate} \end{cases} \tag{40}$$

4.3. Force balance at the contact line

By direct integration of the boundary condition (8), we find that the total restoring elastic stress (a force per unit of length after integration) beneath the contact line (at $x = R$) is given by:

$$f_y^{line} = \gamma_{LV} \sin\theta_{LV} - \gamma_s(\theta_{SL} + \theta_{SV}) \tag{41}$$

Again, this is the macroscopic vertical force balance (2) at the contact lines in the limit of small substrate deflections. Following a calculation similar to that used to obtain equation (41), we can obtain the total elastic stress (force per unit length) integrated over the width of the drop:

$$f_y^{drop} = 2\gamma_s\theta_{SL} - 2\gamma_{LV}\sin\theta_{LV} = 2\gamma_s\left(\theta_{SL} - \theta_{ref}\right) \tag{42}$$

Looking at formula (39), it can be seen that the elastic restoring force f_y^{line} beneath the contact line undergoes a transition for a ratio $l_s/a \sim 1$. In the limit of an infinitely rigid substrate ($l_s/a \to 0$, i.e the sitting mode), the force below the ridge is non-zero and given by $\gamma_{LV}\sin\theta_{LV}$. This is the Young's limit. When the substrate stiffness decreases, the elastocapillary length becomes larger than the width of the contact line, the elastic force decreases and drops to zero when $l_s/a \gg 1$. In this pulling regime, we recover a Neumann-like force equilibrium in which the pulling force exerted at the contact lines is fully balanced by the substrate surface tension. As a consequence, when this regime is reached, further decrease in the substrate stiffness does not increase the height of the substrate deformation at the contact lines, as elastic stresses do not enter the force balance at the corner of the drop. On the other hand, as the substrate stiffness decreases, the depth of the deformation beneath the drop further increases and thus the wet angle increases and the ridge rotates. Equation (42) shows that the when the wet contact angle reaches the value θ_{ref}, the total elastic force beneath the drop vanishes identically. Therefore, in this sinking regime, the forces exerted by the drop on the substrate (by tractions at the contact lines and by the Laplace pressure beneath the drop) are completely balanced solely by the surface tension of the solid substrate.

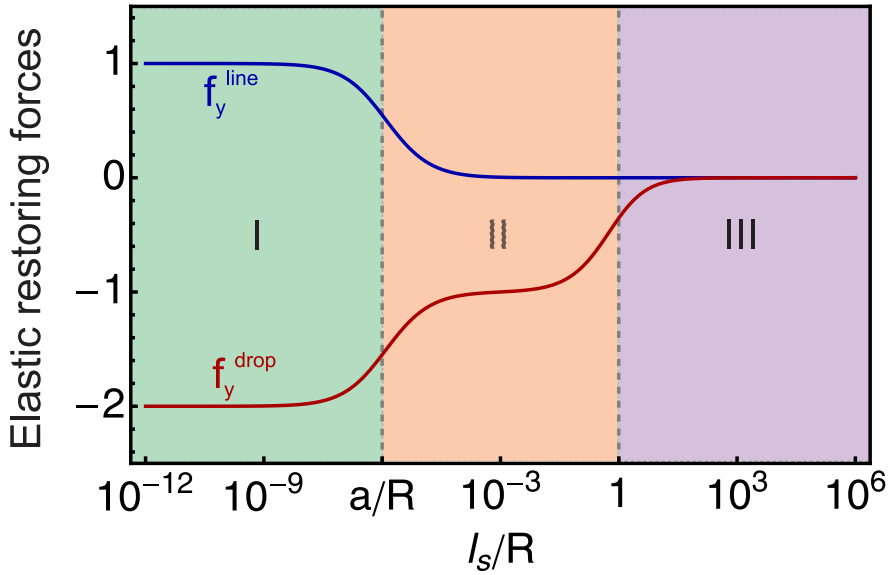

Figure 7: Total elastic force under the contact line (f_y^{line}) and under the drop (f_y^{drop}) as a function of the dimensionless parameter l_s/R. The elastic restoring forces are scaled by $\gamma_{LV}\sin\theta_{LV}$. The Neumann model is recovered in the limit $l_s/R \to \infty$.

4.4. The approximate Green function (slight return)

We now summarize the results for the single and double contact lines using the simplified Green's function introduced previously. In the case of a single contact line with a finite width, the approximate slope $\tilde{\theta}^a(x)$ is given by:

$$\tilde{\theta}^a(x) = -\frac{\Pi_y}{2\pi\mu}\int_{-a}^{a} dy \frac{\text{sign}(x-y)}{|x-y| + 2l_s/\pi} = \theta_{ref}\frac{l_s}{2a\pi}\log\frac{|x-a| + 2l_s/\pi}{|x+a| + 2l_s/\pi} \tag{43}$$

And the approximate slope at the contact line $\tilde{\theta}^a(-a)$ is thus:

$$\tilde{\theta}^a(-a) = \theta_{ref}\frac{l_s}{2a\pi}\log\frac{\pi a + l_s}{l_s} \tag{44}$$

which has the following limits:

$$\tilde{\theta}^a(-a) \sim \theta_{ref}\begin{cases} \dfrac{1}{2}\left(1-\dfrac{a\pi}{2l_s}\right) & \text{soft substrate} \\ \dfrac{l_s}{2a\pi}\log\dfrac{2a}{l_s} & \text{hard substrate} \end{cases} \tag{45}$$

Note that we recover the Neumann regime (i.e $\tilde{\theta}^a(-a) \to \theta_{ref}/2$ when $a/l_s \to 0$) and Young regime (i.e $\tilde{\theta}^a(-a) \to 0$ when $a/l_s \to \infty$). To first order in a/l_s however, the approximate solution (45) differs from the exact solution (23) for the soft substrate. Using the same procedure as for the exact solution, one may compute the slope $\tilde{\theta}^{a2D}(x)$ for a two-dimensional rivulet:

$$\begin{aligned} \tilde{\theta}^{a2D}(x) = &-\frac{\Pi_y}{2\pi\mu}\left\{\int_{-R-a}^{-R+a} \mathrm{d}y \frac{\mathrm{sign}(x-y)}{|x-y|+2l_s/\pi} + \int_{R-a}^{R+a} \mathrm{d}y \frac{\mathrm{sign}(x-y)}{|x-y|+2l_s/\pi}\right\} \\ &+ \frac{P}{2\pi\mu}\int_{-R}^{R} \mathrm{d}y \frac{\mathrm{sign}(x-y)}{|x-y|+2l_s/\pi} \\ &= \theta_{ref}\frac{l_s}{2a\pi}\log\frac{(|x+R-a|+2l_s/\pi)(|x-R-a|+2l_s/\pi)}{(|x+R+a|+2l_s/\pi)(|x-R+a|+2l_s/\pi)} - \theta_{ref}\frac{l_s}{R\pi}\log\frac{|x-R|+2l_s/\pi}{|x+R|+2l_s/\pi} \end{aligned} \tag{46}$$

which lead to the following dry $\tilde{\theta}_{SV} \equiv -\tilde{\theta}^{a2D}(R+a)$ and wet $\tilde{\theta}_{SL} \equiv \tilde{\theta}^{a2D}(R-a)$ approximate contact angles:

$$\tilde{\theta}_{SV} = \theta_{ref}\frac{l_s}{2a\pi}\log\frac{(2a+2l_s/\pi)(2R+2a+2l_s/\pi)}{(2l_s/\pi)(2R+2l_s/\pi)} - \theta_{ref}\frac{l_s}{R\pi}\log\frac{2R+a+2l_s/\pi}{a+2l_s/\pi} \tag{47}$$

$$\tilde{\theta}_{SL} = \theta_{ref}\frac{l_s}{2a\pi}\log\frac{(2a+2l_s/\pi)(2R-2a+2l_s/\pi)}{(2l_s/\pi)(2R+2l_s/\pi)} - \theta_{ref}\frac{l_s}{R\pi}\log\frac{a+2l_s/\pi}{2R-a+2l_s/\pi} \tag{48}$$

For the purpose of comparison with the exact solution given above, it is instructive to extract the asymptotic behaviors of the approximate solution and we find:

$$\theta^a_{SL} - \theta^a_{SV} \sim \frac{\gamma_{LV}\sin\theta}{\gamma_s}\begin{cases} 1-\dfrac{\pi^2R^2}{3l_s^2} & \text{soft substrate} \\ \dfrac{2l_s}{\pi R}\log\dfrac{2R}{l_s} & \text{medium substrate} \end{cases} \tag{49}$$

$$\theta^a_{SL} + \theta^a_{SV} \sim \frac{\gamma_{LV}\sin\theta}{\gamma_s}\begin{cases} 1-\dfrac{\pi a}{2l_s} & \text{medium substrate} \\ \dfrac{l_s}{\pi a}\log\dfrac{a}{l_s} & \text{hard substrate} \end{cases} \tag{50}$$

Although the curves are very similar to the exact ones, there are slight discrepancies in the pulling (medium substrate) and sinking (soft substrate) regime between the exact and approximates solution. Because of their simplicity however, these expressions, as well as the full formula (47)-(48), can be very valuable for the purpose of comparison with experimental data.

5. Selection of the contact angle and conclusion

In this paper, we have first studied the deformation of an incompressible linear elastic substrate by a single contact line. This problem is an extension of the classical problem of Flamant-Cerruti in elasticity [28, 29] but the singular nature of its solution was regularized by the introduction of a finite width $2a$ for the contact line. Depending on the ratio of the elastocapillary length $l_s = \gamma_s/(2\mu)$ over the width of the contact line, two qualitatively distinct regimes have been identified analytically. For $l_s/a \ll 1$, we recover the force balance first described by Young for a drop sitting on a

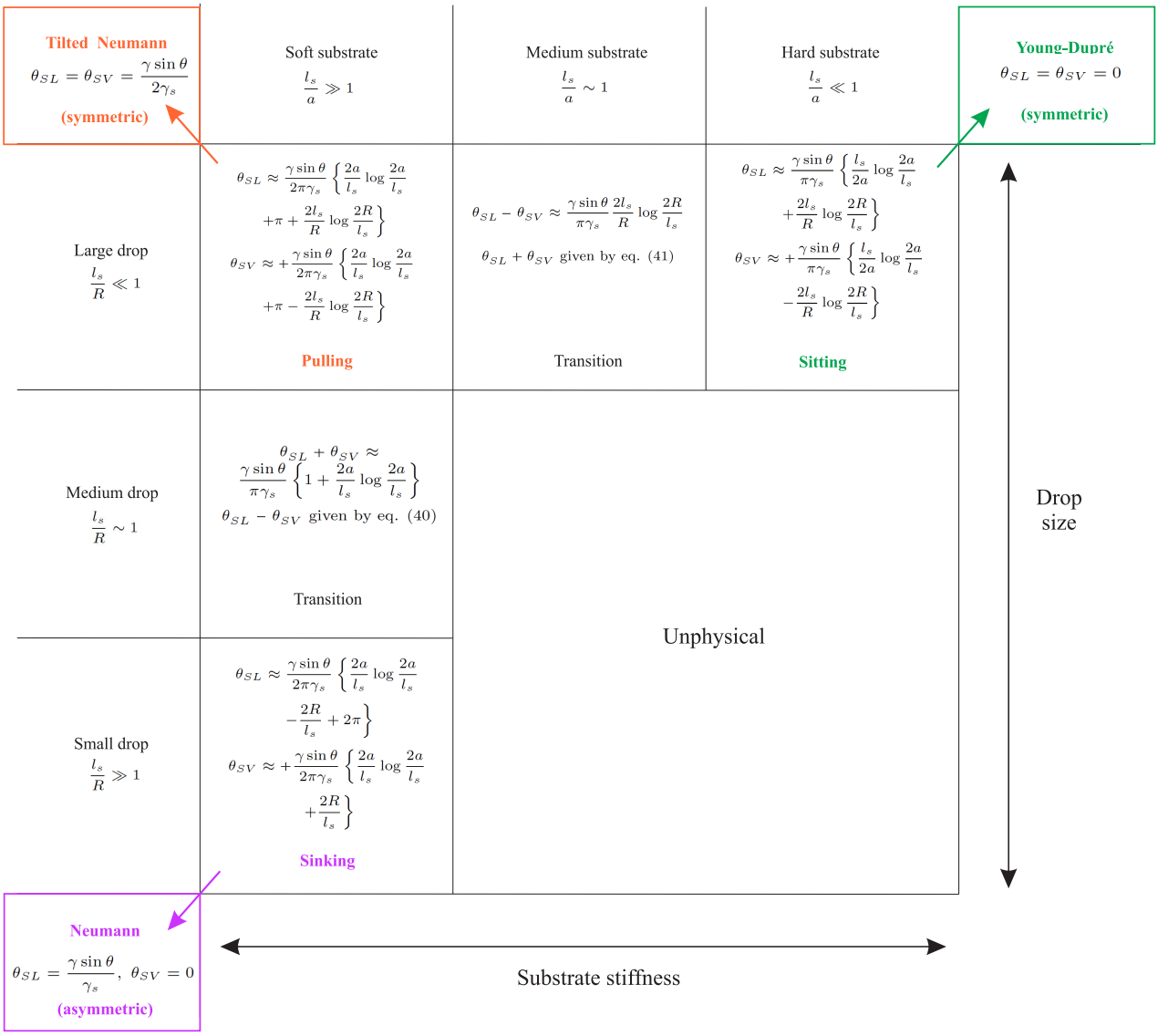

Figure 8: Asymptotic formulas for the substrate deformations at the contact line as a function of the dimensionless ratios l_s/R and l_s/a. The region of the phase diagram where $a \gtrsim R$ is unphysical.

hard substrate while for $l_s/a \gg 1$, we recover a Neumann-like force balance where studied the substrate surface tension balance the pulling force exerted by the contact line. We have then investigated the deformation of an elastic substrate with surface tension by a two-dimensional rivulet of width $2R$. In addition to the forces exerted at the two contact lines, there is additional force on the substrate originating from the Laplace pressure in the rivulet. By analytically solving the equations of equilibrium, we have identified three qualitatively distinct regimes. The transitions between these three regimes are controlled by two dimensionless parameters, l_s/a and l_s/R. For large drops ($R/l_s \gg 1$) resting on hard substrates ($l_s/a \ll 1$), the deformation of the the substrate asymptotically vanishes. In this "sitting" mode, elastic stresses in the substrate balance the tension exerted by the drop at the two contact lines and by the Laplace pressure beneath the drop. For large drop ($R/l_s \gg 1$) on soft substrate ($l_s/a \gg 1$), the substrate is strongly deformed below the contact line. Because the surface of the substrate is deformed, the normal projection of the substrate surface tension is non-zero and exactly balance the vertical traction exerted at the liquid/vapor interface on the solid. In this "pulling" regime, the ridge at the contact line is symmetric and elastic stresses vanish below the contact line. Because elasticity does not contribute to the "macroscopic" force balance at the contact line in this regime, a further decrease

in the substrate stiffness (or if the drop size decrease) does not change the height of the ridge. But since elastic stress must still balance the Laplace pressure below the drop, the depth of the deformation further increase and the ridges below the contact lines "rotate" to accommodate this increase in depth. Finally, in this last regime of small drops ($R/l_s \ll 1$) on soft substrates ($l_s/a \gg 1$), the ridges therefore become asymmetric and the total elastic stress below the drop asymptotically vanishes when the normal projection of the substrate surface tension balances the Laplace pressure in the drop. At this point the total normal elastic stress at the surface of the substrate is zero and the drop is "macroscopically" supported by the surface tension of the solid only. Figure 8 summarizes the formula for the dry and wet angles of the substrate at the contact lines in all three regimes. We now discuss the selection of the contact angle.

In our paper, we have assumed that the contact angle was prescribed and we have calculated the substrate deformations that are induced by a given value of the contact angle. This approach is particularly suited for systems that show an important degree of hysteresis as it is typically the case on deformable substrates [13]. In that situation, the static contact angle is comprised between two values that must be experimentally determined and the substrate deformation can be easily calculated using the results presented in our paper. However, an interesting question arises when one considers a very smooth substrate on which pinning cannot occur. In that case, the contact line will move until it reaches an equilibrium value where the total energy of the system is minimized. In absence of hysteresis, it could be possible, in principle, to predict the value of the contact angle at equilibrium by minimizing the total energy of the system, under the constraint of fixed volume. In our system, the total energy $\mathcal{E}_{tot}$ is given by the sum of the substrate elastic energy as well as the substrate/vapor, substrate/liquid and liquid/vapor interfacial energies or by the following integral:

$$\mathcal{E}_{tot} = \underbrace{\gamma_s \int_{-\infty}^{\infty} \sqrt{1+\left(\frac{\partial \zeta^{a2D}}{\partial x}\right)^2}\,\mathrm{dx}}_{\text{solid-vapour + solid-liquid}} + \underbrace{\gamma_{LV} \int_{-R}^{R} \sqrt{1+\left(\frac{x}{\sqrt{R^2+\frac{R^2}{\tan\theta_{LV}{}^2}-x^2}}\right)^2}\,\mathrm{dx}}_{\text{liquid-vapour}} + \underbrace{\int_{-\infty}^{\infty} \frac{\vec{f}\cdot\vec{u}}{2}\mathrm{dx}}_{\text{elastic energy}} \tag{51}$$

where we have used the fact that the liquid-vapour interface is a portion of spherical cap. The surface displacement field is $\vec{u} = \{u_x^{a2D}(x, y=0), \zeta^{a2D}(x)\}$ (given in appendix) and $\vec{f} = \{f_x, f_y\}$ is the surface traction distribution given by:

$$f_x = \frac{\gamma_{LV}\sin\theta_{LV}}{2a}\Pi\left(\frac{x+R}{2a}\right) + \frac{\gamma_{LV}\sin\theta_{LV}}{R}\Pi\left(\frac{x-R}{2a}\right) - \frac{\gamma_{LV}\sin\theta_{LV}}{R}\Pi\left(\frac{x}{2R}\right) \tag{52}$$

$$f_y = \frac{\gamma_{LV}\cos\theta_{LV}}{2a}\Pi\left(\frac{x+R}{2a}\right) - \frac{\gamma_{LV}\cos\theta_{LV}}{R}\Pi\left(\frac{x-R}{2a}\right) \tag{53}$$

where

$$\Pi(x) = \begin{cases} 1 & |x| < \frac{1}{2} \\ 0 & |x| > \frac{1}{2} \end{cases} \tag{54}$$

This integral was then numerically minimized under the constraint of constant volume and we found an equilibrium angle of $\pi/2$ for all values of the parameters. From the viewpoint of surface energies only, and in the limit of small substrate deformations, the value $\theta_{LV} = \pi/2$ is indeed already a minimum. Therefore, the contact angle can only depart from $\pi/2$ if the increase in surface energies can be compensated by a larger decrease in elastic energy. The numerical minimization reveals that this in fact never happens and the elastic energy is also minimized for vanishing transverse displacements (i.e $\theta_{LV} = \pi/2$), for all values of l_s/R and l_s/a.

While this result is in agreement with the Young-Dupré model for uniform substrate surface tension, it seems rather surprising that it would also applies in the Neumann limit. It is in fact in contradiction with previous work where it was predicted that the liquid-vapour contact angle θ_{LV} should deviate from the value $\pi/2$ in the Neumann limit [7, 24]. This discrepancy in fact stems from the failure of the linear elastic model in the limit where the contact angle $\theta_{LV} \to \pi/2$. Writing $\theta_{LV} = \pi/2 - \epsilon$, one may notice that when ϵ is of order γ_{LV}/γ_S (which is a small parameter), the vertical displacement, which scales as $\gamma_{LV}/\gamma_S \sin\theta_{LV}$, is therefore of order γ_{LV}/γ_S. On the other hand, the tangential displacement, which scales as $\gamma_{LV}/\gamma_S \cos\theta_{LV}$, is therefore of order $(\gamma_{LV}/\gamma_S)^2$. Because of this separation of scales, higher order (nonlinear) terms cannot be neglected in the tangential stress tensor and the slope of the interface must also be taken into account in the boundary conditions. In particular, because the Laplace pressure acts in the direction normal to the interface, there is an additional term $\left(-\frac{\mathrm{d}\zeta}{\mathrm{d}x}\right) \times \left(\gamma_S \frac{\mathrm{d}^2\zeta}{\mathrm{d}x^2}\right)$ on the right hand-side of equation (8). Integrating the tangential stress over the width of the contact line, one thus finds the following total stress f_x^{line}

$$f_x^{line} = \gamma_{LV}\cos\theta_{LV} - \frac{\gamma_s}{2}(\theta_{SV}^2 - \theta_{SL}^2) \tag{55}$$

Because the vertical boundary condition (81) is not affected by nonlinear effects at leading order, we still have:

$$f_y^{line} = \gamma_{LV}\sin\theta_{LV} - \gamma_s(\theta_{SL} + \theta_{SV}) \tag{56}$$

as well as the total vertical stress beneath the drop:

$$f_y^{drop} = 2\gamma_s\left(\theta_{SL} - \theta_{ref}\right) \tag{57}$$

In the Neumann limit of an infinitely soft substrate (i.e when $l_s/R \to \infty$ and $l_s/a \to \infty$), the elastic stresses f_x^{line}, f_y^{line} and f_y^{drop} must vanish and in term of ϵ, equations (55), (56) and (57) now read:

$$\gamma_{LV} = \gamma_s(\theta_{SL} + \theta_{SV}),\ \gamma_{LV}\epsilon = \frac{\gamma_s}{2}(\theta_{SL}^2 - \theta_{SV}^2) \text{ and } \theta_{SL} = \frac{\gamma_{LV}}{\gamma_s} \tag{58}$$

which can be combined to give:

$$\theta_{SL} = \frac{\gamma_{LV}}{\gamma_s},\ \theta_{SV} = 0 \text{ and } \epsilon = \frac{\gamma_{LV}}{2\gamma_s} \tag{59}$$

This result implies that the cusp rotates at the contact line to satisfy the macroscopic Neumann force balance, as described in [24]. In the opposite limit of an infinitely rigid substrate (i.e when $l_s/R \to 0$ and $l_s/a \to 0$), the substrate surface remains flat and the result $\theta_{LV} = \pi/2$ should still hold as nonlinear effect will be negligible. In the intermediate regime of a large drop ($l_s/R \to 0$) on a soft substrate ($l_s/a \to \infty$), the effect of the Laplace pressure on the shape of the ridge is negligible and we expect the ridge to remain symmetric, i.e $\theta_{SL} = \theta_{SV}$ such that equations (55), (56) and (57) reduce to the case studied previously where we found $\theta_{LV} = \pi/2$.

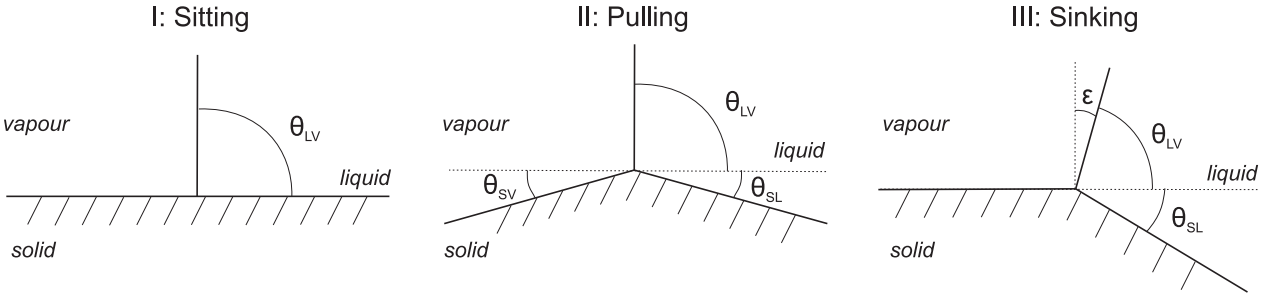

Figure 9: Schematic representations of the substrate deformation at the contact line (far from the microscopic length *a*). Between the pulling and sinking regimes, the apparent contact angle depends on the ratio l_s/R via

In order to go a step further, one may postulate, as in Lubbers et al [24] and in agreement with the numerical calculation performed here to first order in γ_{LV}/γ_S, that the total elastic stresses below the contact line (both tangential and transverse) always vanish at the surface, provided that $l_s/a \gg 1$. This directly leads to the relation: $\gamma_{LV}\cos\theta_{LV} = \frac{\gamma_s}{2}(\theta_{SV}^2 - \theta_{SL}^2)$. By combining this equation with the first equation in (58), one may derive the following relation:

$$\theta_{LV} = \frac{\pi}{2} - \frac{1}{2}(\theta_{SL} - \theta_{SV}) \tag{60}$$

Using the analytical solutions for θ_{SV} and θ_{SL} presented in figure 8, the three angles of interest (ϵ, θ_{SV} and θ_{SL}) can be fully determined for all the values of the physical parameters l_s/R (in the asymptotic limit $l_s/a \to \infty$) without the need to minimize the total energy of the system. The corresponding predictions for the values of the drop contact angles are shown in figure 9. Alternatively, one may derive a simple expression for θ_{LV} by using the approximate solution for $\tilde{\theta}_{SV}$ and $\tilde{\theta}_{SL}$ and we find:

$$\theta_{LV} = \frac{\pi}{2} - \frac{\gamma_{LV}}{2\gamma_s}\left\{\frac{2l_s}{\pi R}\log\left(1 + \frac{\pi R}{l_s}\right) - \frac{l_s}{l_s + \pi R}\right\} \tag{61}$$

While this appears to be a reasonable assumption on a perfectly smooth surface when the contact line can slide and does not transmit tangential stresses, it will nonetheless require a proper derivation using an asymptotic expansion of the displacement field in powers of γ_{LV}/γ_S to infirm or confirm this hypothesis. This is however outside the scope of this paper and will be the subject of future work. On the other hand, most results presented in this paper are directly applicable to the case of strongly hysteretic surfaces for which tangential displacements cannot be neglected, as can indeed be seen in several experimental studies [13, 3].

6. Appendix

6.1. Expression of the displacement field for a single contact line

We give below the analytical expression for the surface displacement field of a substrate loaded by a single contact line

$$\zeta^a(x) = \frac{\Pi_y}{2\pi\mu}\int_{-a}^{a} \mathrm{d}y H(|x-y|) = \frac{\Pi_y}{2\pi\mu} K^a(x) \tag{62}$$

$$u_x^a(x, y=0) = \frac{\Pi_x}{2\pi\mu}\int_{-a}^{a} \mathrm{d}y G(|x-y|) = \frac{\Pi_y}{2\pi\mu} L^a(x) \tag{63}$$

where the functions $K^a(x)$ and $L^a(x)$ are written as:

$$K^a(x), L^a(x) = \begin{cases} K^a_{ext},\, L^a_{ext} & |x| \geq a \\ K^a_{int},\, L^a_{int} & |x| \leq a \end{cases} \tag{64}$$

with the following definitions:

$$\begin{aligned} K^a_{ext}(x) = 2a\left(1 - \frac{x}{a}\mathrm{arctanh}\frac{a}{x}\right) - 2a\log\frac{\sqrt{x^2-a^2}}{\Delta'} + l_s\Bigg(&\mathrm{Ci}\frac{|x|+a}{l_s}\sin\frac{|x|+a}{l_s} - \mathrm{Ci}\frac{|x|-a}{l_s}\sin\frac{|x|-a}{l_s} \\ &- \mathrm{Si}\frac{|x|+a}{l_s}\cos\frac{|x|+a}{l_s} + \mathrm{Si}\frac{|x|-a}{l_s}\cos\frac{|x|-a}{l_s} - \pi\sin\frac{a}{l_s}\sin\frac{|x|}{l_s}\Bigg) \end{aligned} \tag{65}$$

$$\begin{aligned} K^a_{int}(x) = 2a\left(1 + \frac{|x|}{a}\log\sqrt{\frac{a+|x|}{a-|x|}}\right) - 2a\log\frac{\sqrt{a^2-x^2}}{\Delta'} + l_s\Bigg(&\mathrm{Ci}\frac{|x|+a}{l_s}\sin\frac{|x|+a}{l_s} \\ &- \mathrm{Ci}\frac{a-|x|}{l_s}\sin\frac{|x|-a}{l_s} - \mathrm{Si}\frac{|x|+a}{l_s}\cos\frac{|x|+a}{l_s} + \mathrm{Si}\frac{|x|-a}{l_s}\cos\frac{|x|-a}{l_s} + \pi - \pi\sin\frac{a}{l_s}\sin\frac{|x|}{l_s}\Bigg) \end{aligned} \tag{66}$$

$$L^a_{ext}(x) = 2a\left(1 - \frac{x}{a}\mathrm{arctanh}\frac{a}{x}\right) - 2a\log\frac{\sqrt{x^2-a^2}}{\Delta'} \tag{67}$$

$$L^a_{int}(x) = 2a\left(1 + \frac{|x|}{a}\log\sqrt{\frac{a+|x|}{a-|x|}}\right) - 2a\log\frac{\sqrt{a^2-x^2}}{\Delta'} \tag{68}$$

6.2. Expression of the displacement field for the 2D rivulet

Using the notations above, the displacement field for a 2D rivulet on a deformable substrate is given by:

$$\zeta^{a2D}(x) = \frac{\gamma_{LV}\sin\theta_{LV} l_s}{2a\pi\gamma_s} K^a(x-R) + \frac{\gamma_{LV}\sin\theta_{LV} l_s}{2a\pi\gamma_s} K^a(x+R) - \frac{\gamma_{LV}\sin\theta_{LV} l_s}{R\pi\gamma_s} K^R(x) \tag{69}$$

$$u_x^{a2D}(x, y=0) = \frac{\gamma_{LV}\cos\theta_{LV} l_s}{2a\pi\gamma_s} L^a(x-R) + \frac{\gamma_{LV}\cos\theta_{LV} l_s}{2a\pi\gamma_s} L^a(x+R) + \frac{\gamma_{LV}\cos\theta_{LV} l_s}{R\pi\gamma_s} L^R(x) \tag{70}$$

[1] R. Pericet-Camara, A. Best, H.-J. Butt, and E. Bonaccurso, ”Effect of capillary pressure and surface tension on the deformation of elastic surfaces by sessile liquid microdrops: an experimental investigation”, Langmuir 24, 10565 (2008).

[2] E. R. Jerison, Y. Xu, L. A. Wilen, E. R. Dufresne, ”Deformation of an Elastic Substrate by a Three- Phase Contact Line”, Phys. Rev. Lett. 106, 186103 (2011)

[3] T. Kajiya, A. Daerr, L. Royon, T. Narita, F. Lequeux, L. Limat, ”Dynamics of Contact Line of Water Droplets Advancing on Visco-Elastic SBS-Paraffin Gel Substrates”, Soft Matter 9:454-461 (2013).

[4] L. Limat,”Straight contact lines on a soft solid”, EPJ-E, 198103 (2012).

[5] A. Marchand, S. Das, J.H. Snoeijer and B. Andreotti, ”Contact angles on a soft solid: from Young’s law to Neumann’s law”, Phys. Rev. Lett. (2012).

[6] A. Marchand, S. Das, J. H. Snoeijer and B. Andreotti, ”Capillary pressure and contact line force on a soft solid”, Phys. Rev. Lett, 108, 094301 (2012).

[7] R.W. Style and E. R. Dufresne, ”Static wetting on deformable substrates, from liquids to soft solids”, Soft Matter 8, 3177 (2012).

[8] G. R. Lester, ”Contact angles of liquids at deformable solid surfaces”, J. Coll. Sc. 16, 315 (1961).

[9] A. I. Rusanov, ”Theory of wetting of elastically deformed bodies .1. Deformation with a finite contact-angle”, Coll. J. USSR 37, 614 (1975).

[10] M. E. R. Shanahan and P. G. de Gennes, C.R. Acad. Sci. (Paris), 302 (Ser. II), 517 (1986); Adhesion 11, chap. 5, ed by K. W. Allen (London, Elsevier, 1987).

[11] D. Long, A. Ajdari and L. Leibler, ”Static and Dynamic Wetting Properties of Thin Rubber Films”, Langmuir 12, 5221-5230 (1996).

[12] M. E. R. Shanahan, ”The influence of solid micro-deformation on contact angle equilibrium”, J. Phys. D, Appl. Phys, 20, 945-950 (1987).

[13] C. W. Extrand and Y. Kumagai, ”Contact Angles and Hysteresis on Soft Surfaces”, J. Coll. Interface Sc. 184, 191-200 (1996).

[14] D. Szabo, S. Akiyoshi, T. Matsunaga, J. P. Gong, Y. Osada and M. Zrõnyi, ” Spreading of liquids on gel surfaces”, J. Chem. Phys. 13, 18 (2000).

[15] G. Pu and S. J. Severtson, ”Characterization of Dynamic Stick-and-Break Wetting Behavior for Various Liquids on the Surface of Highly Viscous Polymer”, Langmuir, 24, 4685-4692 (2008).

[16] T. Kajiya, P. Brunet, L. Royon, A. Daerr, M. Receveur and L. Limat. ”Liquid Contact Line Receding on a Soft Gel Surface: Dip-Coating Geometry Investigation” Soft Matter, DOI: 10.1039/C4SM01609B (2014).

[17] A. Carré, J.-C. Gastel, M. E. R. Shanahan, ”Viscoelastic effects in the spreading of liquids ”, Nature 379, 432-434 (1996).

[18] K. E. Daniels, S. Mukhopadhyay, P. J. Houseworth, and R. Behringer, ” Instabilities in droplets spreading on gels ”, Phys. Rev. Lett. 99, 124501 (2007).

[19] SJ Park, BM Weon, J San Lee, J Lee, J Kim, JH Je. Visualization of asymmetric wetting ridges on soft solids with X-ray microscopy. Nat Commun. 10;5:4369 (2014).

[20] JB Bostwick, M Shearer, KE Daniels. Elastocapillary deformations on partially-wetting substrates: rival contact-line models. Soft Matter 10: 7361, (2014).

[21] H.-J. Butt, K. Graf, and M. Kappl, Physics and Chemistry of Interfaces, Wiley-VCH (2003).

[22] R. Shuttleworth, ”The Surface Tension of Solids”, Proc. Phys. Soc., London, 63, 444 (1950).

[23] J.H. Weijs, J.H. Snoeijer and B. Andreotti, ”Capillarity of soft amorphous solids: A microscopic model for surface stress”, Phys. Rev. E 89, 042408 (2014).

[24] L.A. Lubbers, J.H. Weijs, L. Botto, S. Das, B. Andreotti and J.H. Snoeijer, ”Drops on soft solids: Free energy and double transition of contact angles”, J. Fluid Mech. 747, R1 (2014).

[25] David, R.; Dobson, S. M.; Tavassoli, Z.; Cabezas, M. G.;Neumann, A. W. Investigation of the Neumann Triangle for Dodecane Liquid Lenses on Water. Colloids Surf., A, 333, 12-18 (2009).

[26] Noblin, X.; Buguin, A.; Brochard-Wyart, F. Fast Dynamics of Floating Triple Lines. Langmuir , 18, 9350-9356 (2002).

[27] J. Sebilleau, Equilibrium Thickness of Large Liquid Lenses Spreading overAnother Liquid Surface, Langmuir (2013)

[28] A. Flamant. Sur la répartition des pressions dans un solide rectangulaire chargé transversalement. Compte. Rendu. Acad. Sci. Paris, vol. 114, p. 1465. (1892).

[29] Cerruti V.: Ricerche intorno all’ equilibrio de’corpi elastici isotropi. R. Accad. Lincei Mem. Cl. Sci. Fis. Mat. e Nat. 3(13), 81-122 (1882)